Springer

KSME

Journal of Mechanical Science and Technology 28 (11) (2014) 4705~4715
www.springerlink.com/content/1738-494x
DOI 10.1007/s12206-014-1037-y

Rarefied gas flow simulations with TMAC in the slip and the transition flow regime using the lattice Boltzmann method †

Namgyun Jeong*

Korea Atomic Energy Research Institute, Daejeon, 305-353, Korea

(Manuscript Received March 17, 2014; Revised August 10, 2014; Accepted August 10, 2014)

Abstract

The lattice Boltzmann (LB) method has been used to simulate rarefied gas flows in micro-systems as an alternative tool, and shown its application possibility. For the rarefied gas flows, the surface roughness plays an important role for the slip phenomenon at the wall. If the wall surface is sufficiently rough, the reflection of the molecules will be diffuse and the tangential momentum accommodation coefficient (TMAC) is equal to unity. However, it has been known that the reflections are not always fully diffuse. In this study, rarefied gas flows are simulated in the slip and the transition flow regime including the effect of the TMAC. For the simulations, new non-fully diffuse wall boundary treatments of the LB method are proposed. The results of 2D and 3D simulations are in excellent agreement with the analytical solutions for the slip flow regime. The solutions of the linearized Boltzmann equation and DSMC for the transition flow regime are compared with those of high order LB method with present boundary conditions, and they are in excellent agreement. The tangential momentum accommodation coefficient effect is also investigated.

Keywords: Lattice Boltzmann method; Micro gas-flow; Slip and transition regime; Tangential momentum accommodation coefficient (TMAC)

1. Introduction

The lattice Boltzmann (LB) method has been recently used to simulate some rarefied gas flows in microsystem [1-5]. The rarefaction effect can be characterized by the Knudsen number Kn, which is the ratio of the mean free path to the characteristic length. Schaaf and Chambre [6] classified different flow regimes based on Kn. For $Kn \leq 0.01$, the fluid can be considered as a continuum, while for $Kn \geq 10$ it is considered a free-molecular flow. Between the two limits with $0.01 < Kn < 10$, which is typical of gas flows in microsystems, the flow is further classified into slip flow for $0.01 < Kn < 0.1$ and transition flow for $0.1 < Kn < 10$. For Kn greater than 0.01, the slip at the solid wall becomes an important flow feature. As the rarefaction effect becomes significant, the pressure drop, shear stress, heat flux, and mass flow rate cannot be properly predicted from the model based on the continuum hypothesis. Unlike conventional numerical schemes which solve the macroscopic variables directly, such as velocity and pressure, the LB method is based on the microscopic kinetic equation for the particle distribution function. Because the LB method is a particle-based method, such as the direct simulation of Monte Carlo (DSMC) method [7], it is applicable to a slip flow. Most importantly, because the LB method deals with particle distribution functions, it is more computationally efficient than the DSMC method.

In the previous slip flow simulations using the LB method, various boundary treatments were applied to obtain the slip velocity at a wall. Among them, bounce-back and specular bounce-back schemes have been widely used. Nie et al. [1] used bounce-back boundary condition for a stationary wall. In the bounce-back scheme, the particle distribution function, which streams to a wall node, scatters back to the node it comes from. However, it is known that it gives less degree of slip at a given Kn [4]. To enhance the slip effect, Succi [2] introduced the specular bounce-back scheme. It is a mix of bounce-back and specular reflections. Lee and Lin [4] used the equilibrium distribution function as a boundary condition. The boundary schemes of those investigations were restricted to fully diffuse flat walls. If the wall surface is sufficiently rough, the reflection of the molecules will be diffuse and the tangential momentum accommodation coefficient (TMAC), σ, is equal to unity, which can be defined for tangential momentum exchange of gas molecules with surfaces, i.e. $\sigma = (\tau_i-\tau_r)/(\tau_i-\tau_w)$, where τ_i and τ_r are the tangential momentum of incoming and reflected molecules, and τ_w is the tangential momentum of re-emitted molecules, corresponding to that of the surface. For most engineering surfaces, it is close to unity. Under controlled test conditions, however, lower accommoda-

*Corresponding author. Tel.: +82 42 868 4524, Fax.: +82 42 861 3642
E-mail address: jng@kaeri.re.kr
† Recommended by Associate Editor Joon Sang Lee

tion coefficients are possible due to the low surface roughness [8]. Sbragaglia and Succi [9] presented a mathematical formulation of kinetic boundary conditions for LB schemes in terms of reflection, slip and accommodation coefficients. In their paper, however, detail investigation and validation using the formula with accommodation coefficient were omitted. Zhang et al. [10] implemented the TMAC to describe the gas-surface interactions in a LB (D2Q9) model. Their boundary condition works in a spirit similar to that of Succi [2]. However, their boundary treatment can only be applied for a stationary wall. Tang et al. [11] presented kinetic theory boundary condition which can be applied for non-fully diffuse wall, and it cannot be adopted only for a stationary wall but also a moving wall. However, it looks somewhat complicated, and it doesn't seem to be easy to use it for a 3D simulation.

The objective of this study is to propose new boundary conditions for non-fully diffuse wall, and to examine the effect of non-unity accommodation on the slip and the transition flows including the compressible effect of gas flow, which has not been considered in the previous studies mentioned above. For the simulations, 2D/3D gas microchannel flows and oscillatory Couette flow are investigated.

2. Slip flow regime (0.01 < *Kn* < 0.1)

2.1 Standard LB method

For a flow without an external force, the following discrete Boltzmann equation is available.

$$\frac{\partial f_\alpha}{\partial t} + e_{\alpha i}\frac{\partial f_\alpha}{\partial x_i} = -\frac{f_\alpha - f_\alpha^{eq}}{\lambda}, \tag{1}$$

where f_α is the particle distribution function, $e_{\alpha i}$ is the microscopic velocity, and λ is the relaxation time. The subscript i corresponds to the respective x, y and z directions. The equilibrium distribution function is given by

$$f_\alpha^{eq} = t_\alpha \rho\left[1 + \frac{e_{\alpha i}u_i}{c_s^2} + \frac{(e_{\alpha i}e_{\alpha j} - c_s^2\delta_{ij})u_i u_j}{2c_s^4}\right], \tag{2}$$

where t_α is a weighting factor, ρ is the density of the system, u_i is the macroscopic velocity, and c_s is the speed of sound. For lattice model, the square lattice (D2Q9) and the 3D 19-velocity (D3Q19) LB models are used for the 2D and 3D simulations, respectively [12].

The D2Q9 model has the following set of discrete velocities:

$$e_\alpha = \begin{cases} 0 & \alpha = 0 \\ (\cos((\alpha-1)\pi/4),\ \sin((\alpha-1)\pi/4)) & \alpha = 1,\ 3,\ 5,\ 7 \\ \sqrt{2}(\cos((\alpha-1)\pi/4),\ \sin((\alpha-1)\pi/4)) & \alpha = 2,\ 4,\ 6,\ 8 \end{cases}, \tag{3}$$

and the weighting factor t_α is

$$t_\alpha = \begin{cases} 4/9 & \alpha = 0 \\ 1/9 & \alpha = 1,\ 3,\ 5,\ 7 \\ 1/36 & \alpha = 2,\ 4,\ 6,\ 8 \end{cases}. \tag{4}$$

For the D3Q19 model, the discrete velocities e_α and the weighting factor t_α are given by

$$e_\alpha = \begin{cases} 0 & \alpha = 0 \\ (\pm 1,\ 0,\ 0),\ (0,\ \pm 1,\ 0),\ (0,\ 0,\ \pm 1) & \alpha = 1,\ 2,\ldots,\ 6;\ \textit{group I} \\ (\pm 1,\ \pm 1,\ 0),\ (\pm 1,\ 0,\ \pm 1),\ (0,\ \pm 1,\ \pm 1) & \alpha = 7,\ 8,\ldots,\ 18;\ \textit{group II} \end{cases} \tag{5}$$

$$t_\alpha = \begin{cases} 12/36 & \alpha = 0 \\ 2/36 & \alpha = 1,\ 2,\ldots,\ 6;\ \textit{group I} \\ 1/36 & \alpha = 7,\ 8,\ldots,\ 18;\ \textit{group II} \end{cases}. \tag{6}$$

The sound speed c_s is $1/\sqrt{3}$ in both 2D and 3D simulations.

By discretizing Eq. (1) along with the characteristic over the time step δt, the following equation can be obtained [9].

$$f_\alpha(\vec{x} + \vec{e}_\alpha \delta t, t + \delta t) - f_\alpha(\vec{x}, t) = -\left.\frac{f_\alpha - f_\alpha^{eq}}{2\tau}\right|_{(\vec{x},t)} - \left.\frac{f_\alpha - f_\alpha^{eq}}{2\tau}\right|_{(\vec{x}+\vec{e}_\alpha\delta t, t+\delta t)}, \tag{7}$$

where the non-dimensional relaxation time $\tau = \lambda/\delta t$.

In the above discretization, the trapezoidal rule is applied to obtain the second-order accuracy and unconditional stability. Using the following modified particle distribution function,

$$\bar{f}_\alpha = f_\alpha + \frac{f_\alpha - f_\alpha^{eq}}{2\tau}. \tag{8}$$

Eq. (7) can be recast in a simpler form as follows.

$$\bar{f}_\alpha(\vec{x} + \vec{e}_\alpha\delta t, t + \delta t) - \bar{f}_\alpha(\vec{x}, t) = -\frac{1}{\tau + 0.5}\left.(\bar{f}_\alpha - f_\alpha^{eq})\right|_{(\vec{x},t)}. \tag{9}$$

The macroscopic density, kinematic viscosity, and momentum are recovered by

$$\begin{aligned} \rho &= \sum_\alpha \bar{f}_\alpha \\ \nu &= \frac{\tau}{3}\frac{\delta x^2}{\delta t} \\ \rho\vec{u} &= \sum_\alpha \vec{e}_\alpha \bar{f}_\alpha \end{aligned}. \tag{10}$$

Hereafter, the overbar on top of the modified distribution function is omitted for simplicity.

For rarefied gas simulations, τ in Eq. (9) needs to be related to Kn. From the kinetic theory, it can be assumed that the gas molecules, represented by the particle distribution functions, travel the distance of the lattice mean-free path l_v with the mean thermal speed defined as $\bar{c} = \sqrt{8kT / \pi m}$ [13] while relaxing to their equilibrium state in the relaxation time λ. The mean thermal speed $\bar{c}$ can be represented with the lattice velocity c which depends on the lattice model [12], e.g., $c = \sqrt{3kT / m}$ for D2Q9 and D3Q19 models.

$$\bar{c} = \sqrt{\frac{8}{3\pi}} c = \sqrt{\frac{8}{3\pi}} \frac{\delta x}{\delta t} . \tag{11}$$

Therefore, the Knudsen number can be expressed as follows [10]:

$$Kn = \frac{l_v}{H} = \frac{\lambda \bar{c}}{H} = \sqrt{\frac{8}{3\pi}} \frac{\lambda}{\delta t} \frac{\delta x}{H} = \sqrt{\frac{8}{3\pi}} \tau \frac{\delta x}{H} , \tag{12}$$

where H is the characteristic length. Because mean free path is inversely dependent on the pressure, the local Kn shall be modified as

$$Kn = Kn_o \frac{P_o}{P(x,y)} , \tag{13}$$

where Kn_o and P_o are the Kn and pressure at the outlet, respectively. The local non-dimensional relaxation time τ is then determined by the local Kn .

2.2 Boundary treatments

2.2.1 Previous boundary conditions

The analytic solution in the Boltzmann equation, the distribution function of the gas molecules leaving the wall surface can be related to the incident molecular distribution function by using a scattering kernel. The most widely used kernel is the diffusive scattering model:

$$\xi(u^i \to u) = \frac{m^2 u_n}{2\pi (kT_w)^2} \exp\left(-\frac{mu^2}{2kT_w} \right) , \tag{14}$$

where u^i is the incident velocity, u the reflected velocity, T_w the surface temperature, and u_n the normal component of the incident velocity. Maxwell [14] expanded this diffusive kernel to a partially diffusive σ and partially specular (1-σ) kernel. In the LB method, the gas molecule and surface interactions need to be approximated by a combination of the discrete velocities, because the degree of freedom in the momentum space is very limited in the LB method.

In order to simulate gas microflows, Zhang et al. [10] and Tang et al. [11] used the Maxwellian approach to describe the gas-solid wall collision characteristics. For 2D channel flow, Zhang et al. [10] presented a boundary condition at the upper as follows:

$$f_8(x,y,t+\delta t) = (1-\sigma) f_2(x-\delta x, y, t) , \tag{15}$$

$$f_6(x,y,t+\delta t) = (1-\sigma) f_4(x+\delta x, y, t) , \tag{16}$$

$$\begin{aligned} f_7(x,y,t+\delta t) &= \sigma f_2(x-\delta x, y, t) + \sigma f_4(x+\delta x, y, t) \\ &\quad + f_3(x,y,t) \end{aligned} , \tag{17}$$

where σ is the TMAC. This boundary condition doesn't include the wall velocity. Their boundary treatment, therefore, can only be applied for a stationary wall.

Tang et al. [11] also suggested the Maxwellian kinetic boundary condition accounting for the TMAC. The unknown distribution function f_α reflected on the wall can be determined by using the incident distribution function $f_{\alpha'}$ and the completely diffusive boundary condition derived by Ansumali and Karlin [15] as follows:

$$\begin{aligned} f_\alpha(\vec{x}, t+\delta t) &= (1-\sigma) f_{\alpha'}(\vec{x}, t+\delta t) \left| (\vec{e}_{\alpha'} - \vec{u}_w) \cdot \vec{n} \right| \\ &\quad + \sigma \frac{\sum_{(\vec{e}_\alpha - \vec{u}_w)\cdot \vec{n} < 0} \left| (\vec{e}_\alpha - \vec{u}_w) \cdot \vec{n} \right| f_\alpha(\vec{x}, t+\delta t)}{\sum_{(\vec{e}_\beta - \vec{u}_w)\cdot \vec{n} > 0} \left| (\vec{e}_\beta - \vec{u}_w) \cdot \vec{n} \right| f_\beta^{eq}(\vec{x}, \rho_w, \vec{u}_w)} f_\alpha^{eq}(\vec{x}, \rho_w, \vec{u}_w) \end{aligned} , \tag{18}$$

where $\vec{u}_w$ and ρ_w are the velocity and density at the wall.

2.2.2 Present boundary conditions

In this study, two different boundary conditions are suggested to simulate rarefied gas flows with non-fully diffuse walls. The first one is a combination of the wall equilibrium and the free-slip boundary conditions. Using the equilibrium distribution function as a boundary condition of the LBE method is to assume that the reflection of molecules impinging on the wall is fully diffuse (σ = 1). On the other hand, free-slip boundary condition [16] applies to the case of smooth boundaries without friction, and it represents a specular reflection (σ= 0), i.e. the incoming particles to the wall are reflected as light is reflected from a mirror after the collision. The non-fully diffuse reflection may lie between these two limits, and the accommodation coefficient, σ, weighs the fraction of diffusive reflection and specular reflection. For 2D case, therefore, the boundary condition at the lower wall is as follows for a non-fully diffuse wall:

$$f_2(x,y,t+\delta t) = \sigma f_2^{eq}(\rho_w, \vec{u}_w, t) + (1-\sigma) f_8(x-\delta x, y+\delta x, t) , \tag{19}$$

$$f_3(x,y,t+\delta t) = \sigma f_3^{eq}(\rho_w, \vec{u}_w, t) + (1-\sigma) f_7(x, y+\delta x, t) , \tag{20}$$

$$f_4(x,y,t+\delta t) = \sigma f_4^{eq}(\rho_w, \vec{u}_w, t) + (1-\sigma) f_6(x+\delta x, y+\delta x, t) . \tag{21}$$

For a stationary wall, $\vec{u}_w$ = 0, and the density is obtained by taking the zeroth moment of the particle distribution function at the wall after the streaming step. Wall boundaries are located halfway between two grid points.

The other boundary condition can be derived by using specular bounce-back scheme for diffusive reflection, which can be presented as follows:

$$f_2(x,y,t) = rf_6(x,y,t) + (1-r)f_8(x,y,t) , \quad (22)$$
$$f_3(x,y,t) = f_7(x,y,t) , \quad (23)$$
$$f_4(x,y,t) = rf_8(x,y,t) + (1-r)f_6(x,y,t) , \quad (24)$$

where r is the specular factor. The sum of x-momentum for re-emitted particles from the bottom wall after the collision is as follows:

$$J_x = f_2 - f_4 = (1-2r)(f_8 - f_6) = \frac{\rho}{6}u_w , \quad (25)$$

and

$$r = \frac{1}{2} - \frac{\rho}{12}\frac{u_w}{f_8 - f_6} . \quad (26)$$

If a stationary wall is considered, r should be 0.5, and J_x becomes 0, which means diffuse reflection, i.e. the particles reflected back diffusively from the wall without a certain angle of reflection. Thus, non-fully diffuse reflection can be possibly achieved by following boundary condition:

$$f_2(x,y,t) = r\sigma f_6(x,y,t) + (1-r\sigma)f_8(x,y,t) , \quad (27)$$
$$f_3(x,y,t) = f_7(x,y,t) , \quad (28)$$
$$f_4(x,y,t) = r\sigma f_8(x,y,t) + (1-r\sigma)f_6(x,y,t) . \quad (29)$$

Wall boundaries are also located halfway between two grid points.

2.3 Numerical simulation

2.3.1 2D microchannel flow

The analytic solution of a microchannel flow between two parallel plates of length L, which are separated apart by a distance H, can be deduced from the Navier-Stokes equation using the slip boundary condition. When the second-order slip model is considered, the slip velocity is

$$u_s - u_{wall} = \alpha\frac{2-\sigma}{\sigma}l\left.\frac{\partial u}{\partial n}\right|_{wall} - \beta l^2\left.\frac{\partial^2 u}{\partial n^2}\right|_{wall} , \quad (30)$$

where u_s and n are the slip velocity and wall normal coordinate, and u_{wall} denotes the wall velocity. For a flat wall, Hadjiconstantinou [17] has been proposed the slip coefficients α = 1.11 and β = 0.61 from the accurate numerical solutions of the Boltzmann equation. Under the assumption of a long channel, i.e. L/H >> 1, the following analytical solutions can be deduced with Eq. (30) [18].

velocity:

$$u(y) = -\frac{H^2}{2\mu}\frac{dP}{dx}\left[-\left(\frac{y^2}{H^2}\right)+\left(\frac{y}{H}\right)+1.11\frac{2-\sigma}{\sigma}Kn + 2\times 0.61Kn^2\right], \quad (31)$$

pressure:

$$1-\tilde{P}^2 + 12\times 1.11\frac{2-\sigma}{\sigma}Kn_o(1-\tilde{P}) - 24\times 0.61Kn_o^2\ln\tilde{P} = B(1-\tilde{x}) , \quad (32)$$

where R is the gas constant; $\tilde{P} = P/P_o$, the normalized pressure with the outlet pressure; $\tilde{x} = x/L$, the coordinate normalized with the channel length; and B a constant such that $\tilde{P}(0) = P_i/P_o$.

The unknown particle distribution functions at the inlet and outlet are calculated by second-order extrapolation of those adjacent to the boundary nodes. Following the extrapolation, the calculated densities at the inlet and outlet are rescaled to make the average density across the inlet and outlet boundary nodes the same as the prescribed density.

Fig. 1 shows the results for Kn_o = 0.05, 0.1 and σ = 0.9, 0.6 compared with the analytical solutions of Eqs. (31) and (32). The grid size for H is restricted to $30\delta x$ (32 points), and L/H = 80 is used in order to investigate the compressibility and rarefaction effects on a sufficiently long micro-channel flow. For all calculations, P_i/P_o is set to 2.0. The nonlinearity of pressure, i.e. deviation of the pressure from the linear pressure distribution, $(P - P_{incomp.})$, is normalized by the outlet pressure, P_o, and the stream direction, in an x coordinate, is normalized by the channel length. Slip velocities are normalized by the outlet centerline velocity U_o. The results are same for both boundary treatments, and they are also in excellent agreement with the analytical solutions. That shows that non-fully diffuse reflection can be successfully achieved by linear combination of fully diffuse and specular reflections, and the wall equilibrium boundary condition and the specular bounce-back scheme with r = 0.5 represent the diffuse reflection well.

For the comparison with the previous boundary treatments, the results for Kn_o = 0.1 and σ = 0.9 are presented in Fig. 2. The results of previous boundary treatments show lower values of the slip velocity and nonlinearity of pressure when compared with the analytical solutions.

To evaluate the effect of grid size on the accuracy of the solutions, the gas flows in an infinitely long microchannel are studied.

In order to mimic the flow, a periodic microchannel flow driven by a constant external pressure gradient is considered. In the presence of a body force, the LB must be modified to account for the force by adding an additional term to Eq. (9). The simplest way with body force density $\vec{F} = \rho\vec{g}$, where $\vec{g}$ is the acceleration, is as follows [19]:

$$\bar{f}_\alpha(\vec{x} + \vec{e}_\alpha\delta t, t + \delta t) - \bar{f}_\alpha(\vec{x},t) = -\frac{1}{\tau + 0.5}\left.(\bar{f}_\alpha - f_\alpha^{eq})\right|_{(\vec{x},t)} + \delta t F_\alpha , \quad (33)$$

where

$$F_\alpha = \left(1 - \frac{1}{2\tau + 1}\right)t_\alpha\left[\frac{\vec{e}_\alpha - \vec{u}}{c_s^2} + \frac{(\vec{e}_\alpha\cdot\vec{u})}{c_s^4}\vec{e}_\alpha\right]\cdot\vec{F} . \quad (34)$$

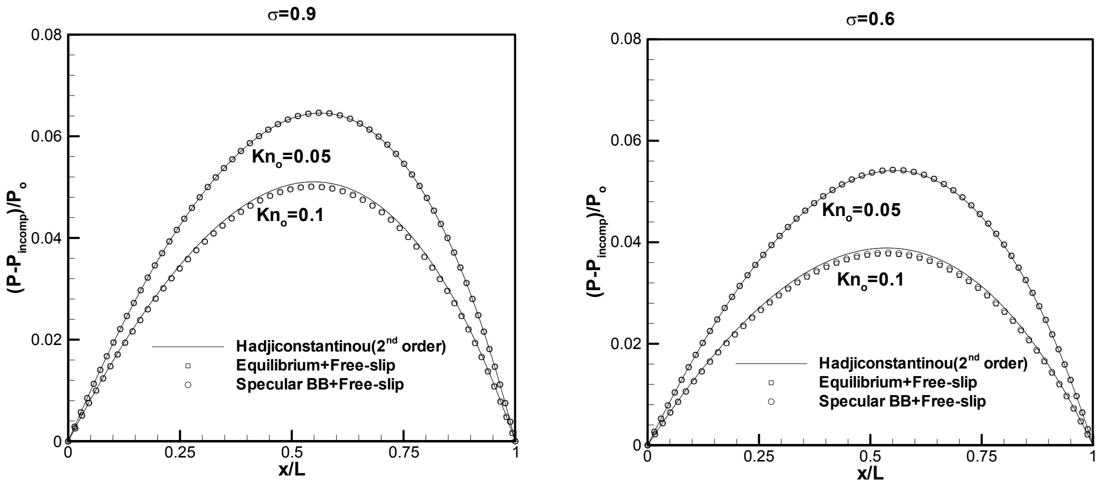

(a) Nonlinearity of pressure normalized by the outlet pressure

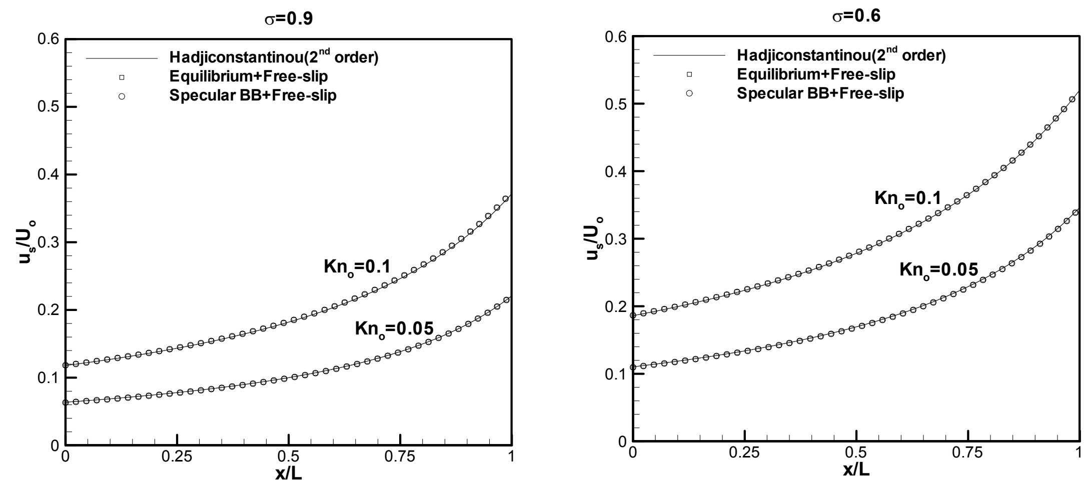

(b) Slip velocity normalized by the outlet centerline velocity

Fig. 1. Nonlinearity of pressure and slip velocity distributions for Kn_o = 0.05, 0.1 and σ = 0.9, 0.6 at P_i/P_o = 2.0, H = 30δx, and L/H = 80.

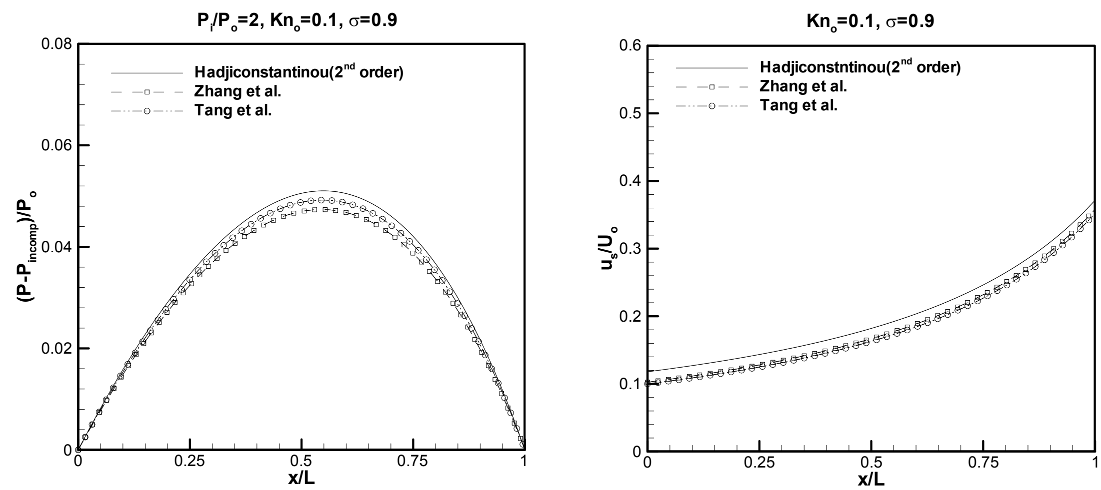

(a) Nonlinearity of pressure normalized by the outlet pressure (b) Slip velocity normalized by the outlet centerline velocity

Fig. 2. Nonlinearity of pressure and slip velocity distributions of previous boundary treatments for Kn_o = 0.1 and σ = 0.9.

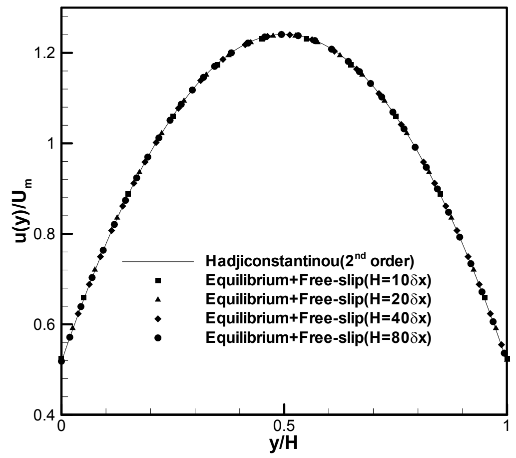

(a) Combination of wall equilibrium and free-slip condition

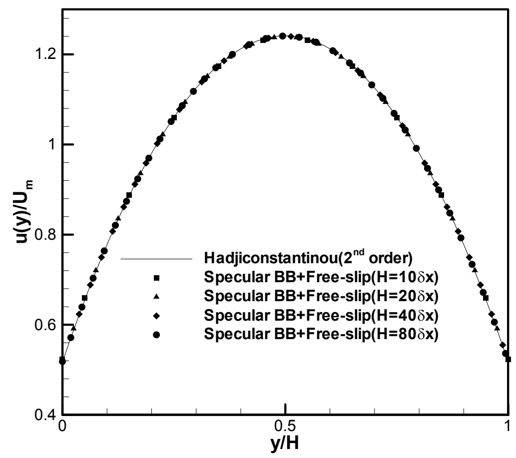

(b) Combination of specular bounce-back and free-slip condition.

Fig. 3. Non-dimensional velocity profiles for the cases of $H = 10\delta x$, $20\delta x$, $40\delta x$, and $80\delta x$ when $Kn = 0.1$ and $\sigma = 0.8$.

For the external pressure gradient, $F_x = -\partial P / \partial x$ is applied.

Fig. 3 shows the velocity profiles for the cases of $H = 10\delta x$, $20\delta x$, $40\delta x$, and $80\delta x$ when $Kn = 0.1$ and $\sigma = 0.8$. The results are non-dimensionalized by the mean velocity U_m,

$$U_m = -\frac{H^2}{2\mu}\frac{dP}{dx}\left[\frac{1}{6} + 1.11\frac{2-\sigma}{\sigma}Kn + 2\times 0.61 Kn^2\right]. \quad (35)$$

It is seen that the accuracy of the solutions is essentially independent of the grid size for both boundary conditions.

2.3.2 Oscillatory shear-driven gas flow

The schematic diagram of the oscillatory Couette flow is presented in Fig. 4. The lower plate at $y = 0$ is a stationary wall and the upper plate at $y = H$ is a moving wall. At time $t = 0$, the upper plate starts to oscillate in the x direction with velocity $u = u_w sin(\omega t)$. ω is the oscillation frequency and u_w is the velocity amplitude.

Oscillatory Couette flow is characterized by the Stokes

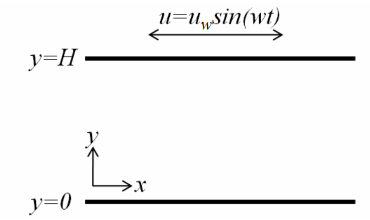

Fig. 4. Schematic diagram of the oscillatory Couette flow.

number S, which represents balance between the unsteady and viscous effects, defined as $S = \sqrt{\omega H^2 / \nu}$. The reduced Navier-Stokes equation for the Couette flow problem is $\partial u / \partial t = \nu \partial^2 u / \partial y^2$, and boundary conditions for oscillatory rarefied flow are as follows:

at $y = 0$:

$$u = \alpha\frac{2-\sigma}{\sigma} l \frac{\partial u}{\partial y} - \beta l^2 \frac{\partial^2 u}{\partial y^2} \quad (36)$$

at $y = H$:

$$u - u_w \,\mathrm{Im}[\exp(i\omega t)] = -\alpha\frac{2-\sigma}{\sigma} l \frac{\partial u}{\partial y} + \beta l^2 \frac{\partial^2 u}{\partial y^2}. \quad (37)$$

The solution is then given by [20]

$$u(y) = \mathrm{Im}\left\{\left[A\cosh\left(\xi\frac{H-y}{H}\right) + B\sinh\left(\xi\frac{H-y}{H}\right)\right]\exp(i\omega t)\right\}, \quad (38)$$

where

$$A = u_w \frac{C_2}{\left(1+\beta\xi^2 Kn^2\right)C_2 + \alpha\frac{2-\sigma}{\sigma}\xi Kn C_1} \quad (39)$$

$$B = -\frac{C_1}{C_2}A \quad (40)$$

$$C_1 = \cosh\xi + \alpha\frac{2-\sigma}{\sigma}\xi Kn\cdot\sinh\xi + \beta\xi^2 Kn^2\cosh\xi \quad (41)$$

$$C_2 = \sinh\xi + \alpha\frac{2-\sigma}{\sigma}\xi Kn\cdot\cosh\xi + \beta\xi^2 Kn^2\sinh\xi \quad (42)$$

and $\xi = \sqrt{i}S$.

The periodic boundary condition is applied in the x direction. The oscillation frequency can be related with non-dimensional period T_p as $\omega = 2\pi/(T_p\delta t)$. In Fig. 5, the comparison of the dynamic velocity profiles for $\sigma = 0.9$; $\sigma = 0.5$, and $Kn = 0.05$; $Kn = 0.1$ is shown. For all calculations, S is fixed to 4.0. It is seen that the present results are in excellent agreement with those of analytical solutions. In addition, the symbols which represent the results of two boundary treatments are located on the same positions.

2.3.3 3D microchannel flow

In order to examine that the present boundary treatments are

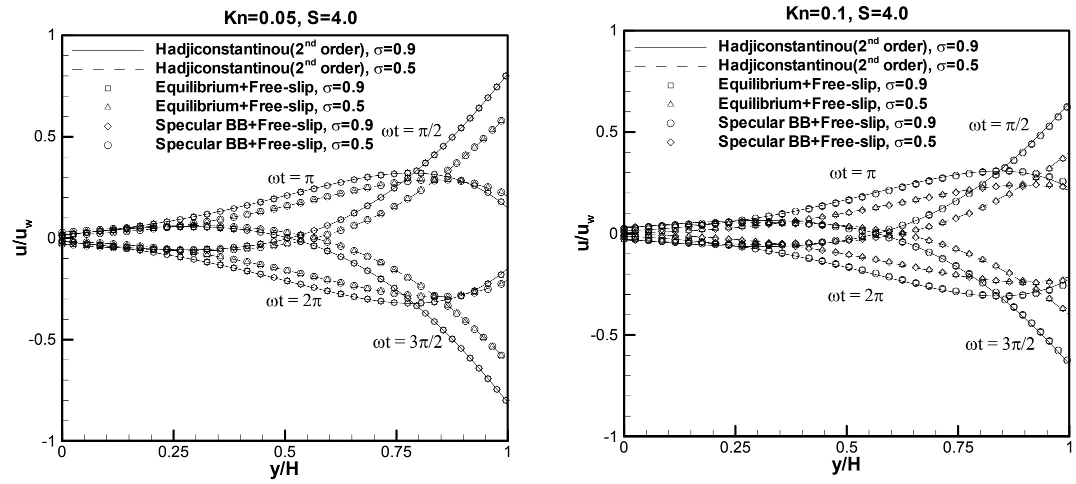

(a) $Kn = 0.05$ and $S = 4.0$ (b) $Kn = 0.1$ and $S = 4.0$

Fig. 5. Non-dimensional dynamic velocity profiles for $\sigma = 0.9$; $\sigma = 0.5$, and $Kn = 0.05$; $Kn = 0.1$.

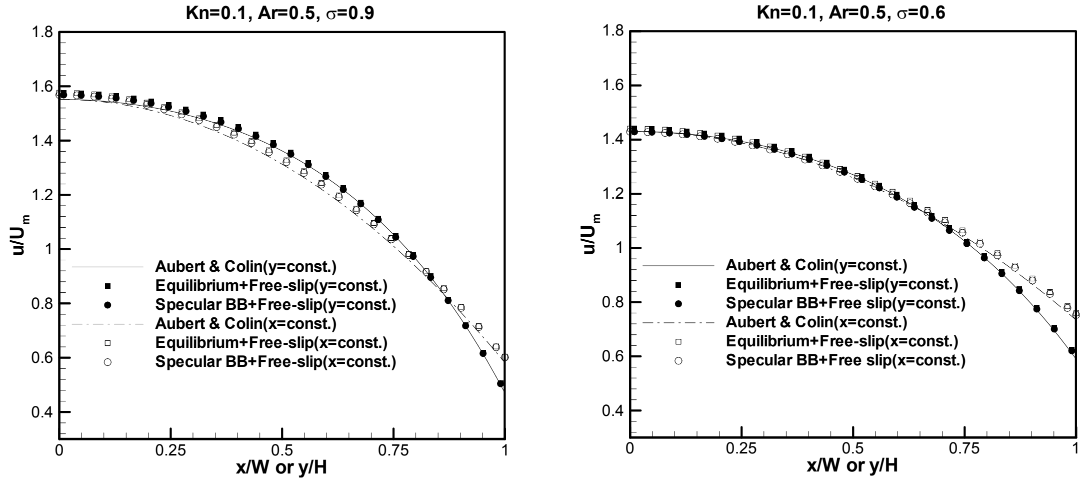

(a) $\sigma = 0.9$ (b) $\sigma = 0.6$

Fig. 6. Non-dimensional velocity profile of 3D microchannel flow for $Kn = 0.1$ and $Ar = 0.5$.

also applicable in a 3D simulation, 3D gas microchannel flow is simulated. The length of the channel is L, its width is $2W$, and its depth is $2H$, so that $z \in \{0, L\}$, $x \in \{-W, W\}$, and $y \in \{-H, H\}$. The aspect ratio of the cross section is $Ar = H/W$, and it is assumed that $H <= W$. Under the assumption of a long channel, i.e. $W, H << L$, and a locally fully developed flow, i.e. the density ρ and the pressure P are constant within a cross section, the steady compressible gas flow in a cross section is governed by the conservation and momentum equations:

$$\frac{\partial u}{\partial z} = 0 \tag{43}$$

$$\frac{\partial^2 u}{\partial y^2} + \frac{\partial^2 u}{\partial x^2} = \frac{1}{\mu}\frac{dP}{dz}. \tag{44}$$

For the simulation of infinitely long channel, Eq. (33) and periodic boundary condition in z direction are applied.

Fig. 6 shows the velocity profiles non-dimensionalized by the mean velocity, $U_m = \frac{1}{A}\int_A u(x,y)dA$, for $Kn = 0.1$ and $Ar = 0.5$. Two cases of $\sigma = 0.9$ and 0.6 are considered to see the non-unity accommodation effect. The results are compared with those of the analytical solution derived by Aubert and Colin [21]. They presented the solution based on a double Fourier series using the second-order slip model proposed by Deissler [22]. The results of present study are in very good agreement with the analytical solutions even for the case of quite smooth wall. The deviation between the results of two boundary conditions is negligible.

The simulations for a long 3D microchannel, which has finite length, are also carried out. $400\delta x$, $20\delta x$, and $10\delta x$ are used for L, W and H, respectively. Figs. 7(a) and (b) show the velocity contours at the side wall and bottom wall when $Kn_o = 0.1$, and $\sigma = 0.9$; $\sigma = 0.6$, respectively. The slip velocity at the

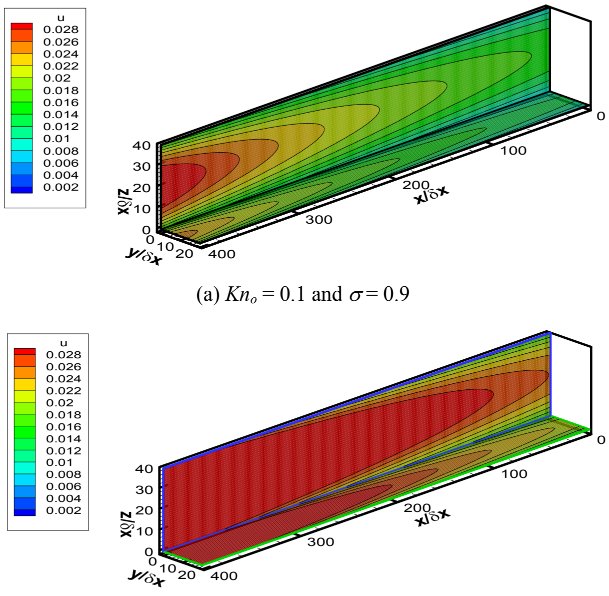

(a) $Kn_o = 0.1$ and $\sigma = 0.9$

(b) $Kn_o = 0.1$ and $\sigma = 0.6$

Fig. 7. Velocity contours at the side wall and bottom wall of a long 3D microchannel.

side wall becomes larger than that of bottom wall. The difference comes from variation in the shear rate along the walls. Consequently, the slip velocity distribution in 3D gas microchannel flow is much more complicated than its 2D counterpart, which assumes the velocity profile to be a simple combination of a parabolic velocity profile and a known slip velocity.

3. Transition flow regime (0.1 < *Kn* < 1)

3.1 High order LB method

When the Knudsen number becomes larger than 0.1, the real velocity profile distinctly deviates from the one predicted by the standard LB model because of the Knudsen layer effect near the wall. To capture the flow characteristics in the Knudsen layer, high order LB model should be adopted. Tang et al. [23] showed following D2Q13 model can predict flow in the transition regime.

$$f_\alpha^{eq} = t_\alpha \rho \left[1 + \frac{e_{\alpha i} u_i}{c_s^2} + \frac{(e_{\alpha i} u_i)^2}{2c_s^4} - \frac{u_i u_i}{2c_s^2} + \frac{(e_{\alpha i} u_i)^3}{2c_s^6} - \frac{3(e_{\alpha i} u_i)(u_i u_i)}{2c_s^4} \right] \tag{45}$$

where $c_s^2 = c^2/2$ and $c = \sqrt{2RT}$.

The D2Q13 model has the following set of discrete velocities:

$$e_\alpha = \begin{cases} 0 & \alpha = 0 \\ (\cos((\alpha-1)\pi/4),\ \sin((\alpha-1)\pi/4)) & \alpha = 1,\ 3,\ 5,\ 7 \\ \sqrt{2}(\cos((\alpha-1)\pi/4),\ \sin((\alpha-1)\pi/4)) & \alpha = 2, 4,\ 6,\ 8 \\ 2(\cos((\alpha-1)\pi/4),\ \sin((\alpha-1)\pi/4)) & \alpha = 9, 10, 11, 12 \end{cases} \tag{46}$$

and the weighting factor t_α is

$$t_\alpha = \begin{cases} 3/8 & \alpha = 0 \\ 1/12 & \alpha = 1,\ 3,\ 5,\ 7 \\ 1/16 & \alpha = 2,\ 4,\ 6,\ 8 \\ 1/96 & \alpha = 9, 10, 11, 12 \end{cases} . \tag{47}$$

To consider the Knudsen layer effect, the local relaxation time should be determined, and can be related with the local mean free path as follows [24]:

$$\tau = \frac{l}{l_o}\sqrt{\frac{\pi}{8}}\frac{c}{c_s} Kn \frac{H}{\delta x}, \tag{48}$$

where l_o and l are the macroscopic property based mean free path and the local mean free path. For the gas flow between two parallel plates at $y = 0$ and $y = L$, the local mean free path of the molecules can be calculated as follows:

$$l(y) = l_o \left[1 + (\varphi - 1)\exp(-\varphi) - \varphi^2 \int_\varphi^\infty t^{-1} \exp(-t)\, dt \right], \tag{49}$$

where $\phi = y/l_o$ for the molecules moving towards $y = 0$ and $\phi = (L-y)/l_o$ for moving towards $y = L$. The local mean free path of all molecules can be determined by averaging these two parts, because a molecule can move towards either side of the walls with equal probability. For $y = 0$ or $y = L$, $\phi = L/l_o$ can be used.

3.2 Boundary treatments

For the case of the combination of the wall equilibrium and the free-slip boundary conditions, only the information of the particle distribution function f_{10} needs to be added in the Eqs. (19)-(21). For high order LB method, therefore, the boundary condition at the lower wall is as follows:

$$f_2(x,y,t+\delta t) = \sigma f_2^{eq}(\rho_w, \vec{u}_w, t) + (1-\sigma) f_8(x-\delta x, y+\delta x, t), \tag{50}$$

$$f_3(x,y,t+\delta t) = \sigma f_3^{eq}(\rho_w, \vec{u}_w, t) + (1-\sigma) f_7(x, y+\delta x, t), \tag{51}$$

$$f_4(x,y,t+\delta t) = \sigma f_4^{eq}(\rho_w, \vec{u}_w, t) + (1-\sigma) f_6(x+\delta x, y+\delta x, t), \tag{52}$$

$$f_{10}(x,y,t+\delta t) = \sigma f_{10}^{eq}(\rho_w, \vec{u}_w, t) + (1-\sigma) f_{12}(x, y+2\delta x, t). \tag{53}$$

The other boundary condition can be derived in similar way of the standard LB method except the specular factor. The specular factor, r, should be recalculated from the sum of x-momentum for re-emitted particles from the bottom wall as follows:

$$J_x = f_2 - f_4 = (1-2r)(f_8 - f_6) = \frac{\rho}{4} u_w (1 - u_w), \tag{54}$$

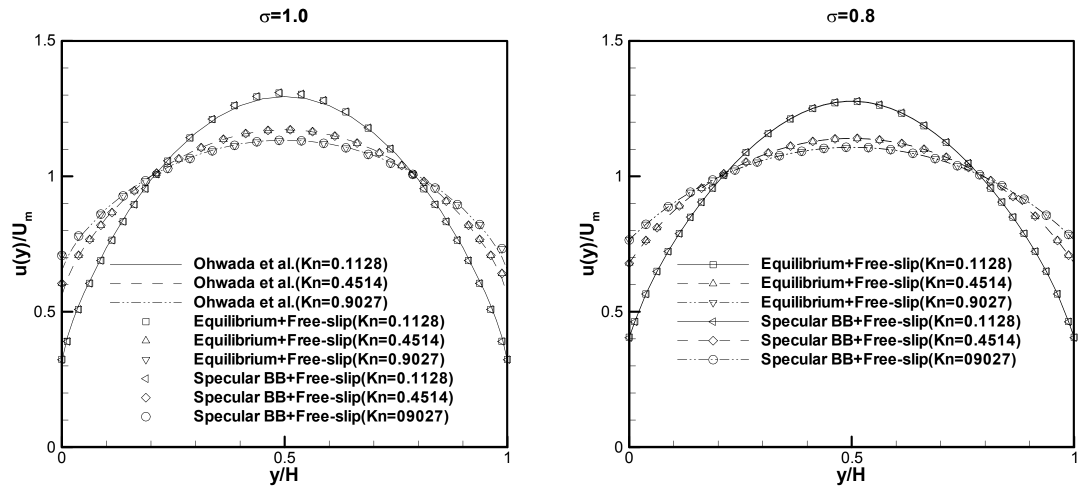

(a) $\sigma = 1.0$ (b) $\sigma = 0.8$

Fig. 8. Non-dimensional velocity profiles for Poiseuille flow at Kn = 0.1128, 0.4514, and 0.9027.

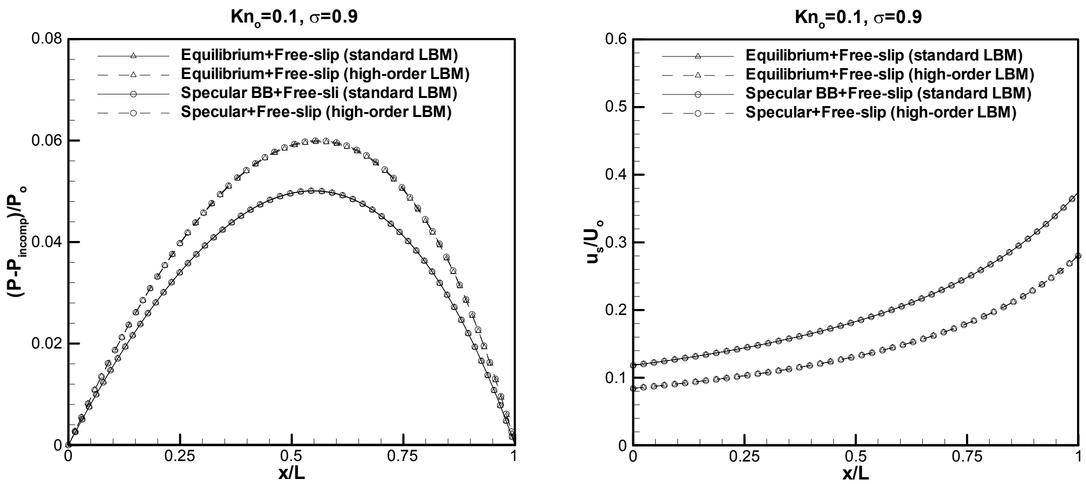

(a) Nonlinearity of pressure normalized by the outlet pressure (b) Slip velocity normalized by the outlet centerline velocity

Fig. 9. LB model comparison of nonlinearity of pressure and slip velocity distributions for Kn_o = 0.1 and σ = 0.9.

and

$$r = \frac{1}{2} - \frac{\rho}{8}\frac{u_w(1-u_w)}{f_8 - f_6}. \tag{55}$$

Thus, non-fully diffuse reflection can be possibly achieved by following boundary condition:

$$f_2(x,y,t) = r\sigma f_6(x,y,t) + (1-r\sigma) f_8(x,y,t) , \tag{56}$$

$$f_3(x,y,t) = f_7(x,y,t) , \tag{57}$$

$$f_4(x,y,t) = r\sigma f_8(x,y,t) + (1-r\sigma) f_6(x,y,t) , \tag{58}$$

$$f_{10}(x,y,t) = f_{12}(x,y,t) . \tag{59}$$

3.3 Numerical simulation

For the comparison with the solution of the linearized Boltzmann equation obtained by Ohwada et al. [25], the simulations of gas flows in an infinitely long microchannel are carried out. Fig. 8 shows the nondimensional velocity profiles for Poiseuille flow at Kn = 0.1128, 0.4514, and 0.9027. It is seen that the accurate results that are close to the direct solution of the Boltzmann equation can be obtained by high order LB method with the present boundary conditions. The results for σ = 0.8 are also presented in the figure.

To examine the Knudsen layer effect on the slip velocity, the long microchannel gas flows are simulated. The grid size for H is restricted to $30\delta x$ (32 points), and L/H = 80 is used as for the standard case. P_i/P_o is set to 2.0. Fig. 9 shows the nonlinearity of the pressure and the slip velocity along the stream direction for Kn_o = 0.1 and σ = 0.9. When compared with the solutions obtained by the standard LB method, it is observed that the nonlinearity of the pressure increases, and the slip velocity along the wall decreases when the Knudsen layer

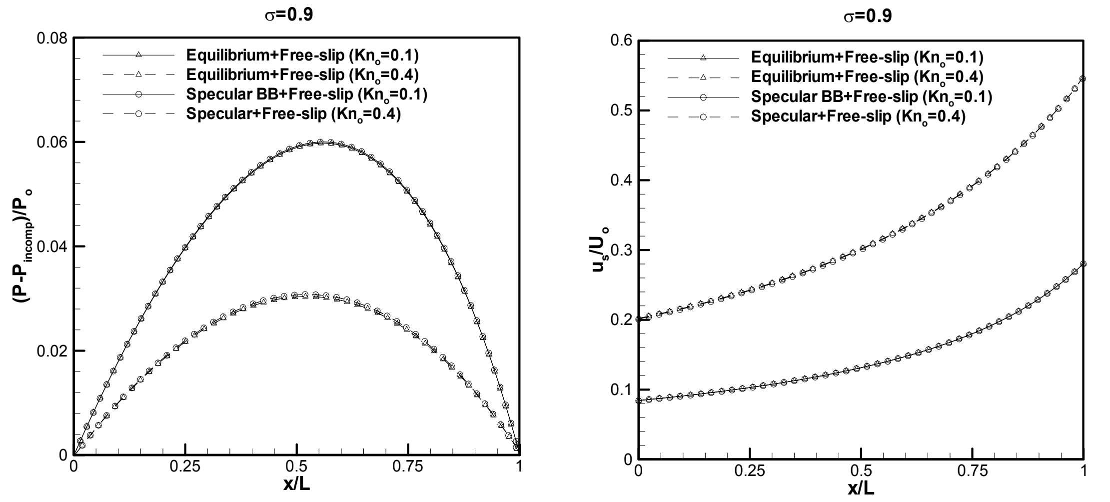

(a) Nonlinearity of pressure normalized by the outlet pressure (b) Slip velocity normalized by the outlet centerline velocity

Fig. 10. Nonlinearity of pressure and slip velocity distributions for Kn_o = 0.4 and σ = 0.9.

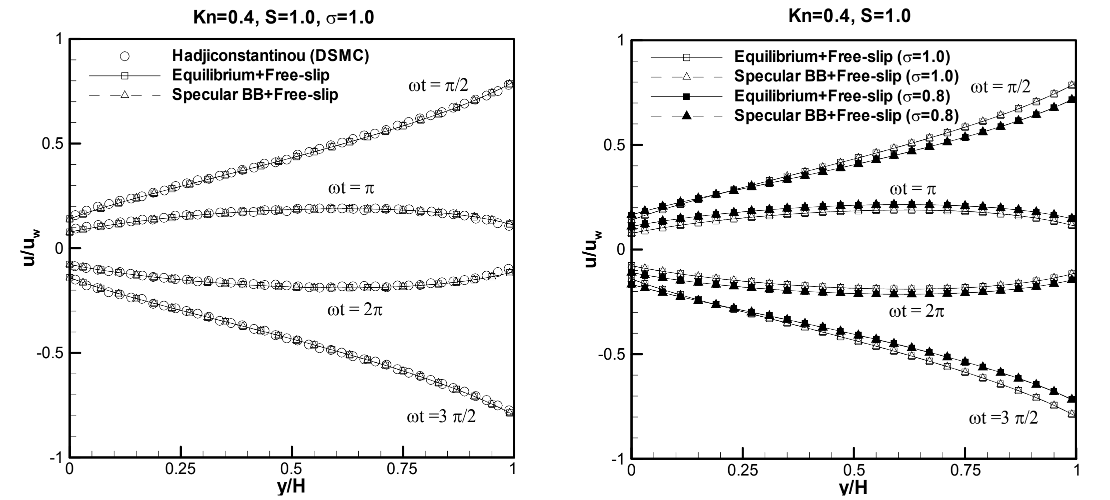

(a) σ = 1.0 (b) σ = 0.8

Fig. 11. Non-dimensional the dynamic velocity profiles for Kn = 0.4 and S = 1.0.

effect is considered. In Fig. 10, the results of Kn_o = 0.4 and σ = 0.9 are plotted. As the Knudsen number increases, the nonlinearity of the pressure decreases, and the slip velocity gets larger.

Finally, oscillatory Couette flow is also calculated to find out whether the present boundary conditions are available for transitional flow with a moving wall. Fig. 11(a) compares the dynamic velocity profiles for Kn = 0.4 and S = 1.0 from the high order LB method with present boundary conditions against the DSMC data [20]. It is seen that the velocity profiles are in excellent agreement with DSMC results even in the Knudsen layer. In Fig. 11(b), the results for σ = 0.9 are illustrated to see the tangential moment accommodation coefficient effect.

4. Conclusions

In this study, rarefied gas flows are simulated in the slip and the transition flow regime. In the simulations, the effect of the TMAC is considered. For the boundary treatment of non-fully diffuse wall, two new boundary conditions, which achieve the non-fully diffuse reflection by a linear combination of the diffuse and specular reflection, are proposed. For the specular reflection, free-slip boundary condition is used, and the wall equilibrium and specular bounce-back schemes are used for the diffuse reflection. The TMAC, σ, weighs the fraction of diffusive reflection and specular reflection. For the slip flow simulations, 2D/3D microchannel flows and oscillatory shear-driven gas flow are considered, and the results are in excellent agreement with the analytic solutions. To investigate the Knudsen layer effect, high order LB method is applied, and the present boundary conditions are slightly modified. It is found out that present boundary treatments are also applicable for the simulations of transition flow.

Nomenclature

Kn : Knudsen number
e_α, $e_{\alpha i}$: Discrete velocity, microscopic velocity
f_α : Particle distribution function
f_α^{eq} : Equilibrium particle distribution function
$\vec{u}$: Macroscopic velocity
ν : Kinematic viscosity
τ : Non-dimensional relaxation time
l_v : Viscosity-based mean free path
l : Local mean free path
σ : Tangential momentum accommodation coefficient

References

[1] X. Nie, G. D. Doolen and S. Chen, Lattice-Boltzmann Simulations of Fluid Flows in MEMS, *J. Stat. Phys.,* 107 (2002) 279-289.
[2] S. Succi, Mesoscopic modeling of slip motion at fluid-solid interfaces with heterogeneous catalysis, *Phys. Rev. Lett.,* 89 (2002) 064502.
[3] C. Y. Lim, C. Shu, X. D. Niu and Y. T. Chew, Application of lattice Boltzmann method to simulate microchannel flows, *Phys. Fluids,* 14 (2002) 2299-2308.
[4] T. Lee and C. L. Lin, Rarefaction and compressibility effects of the lattice Boltzmann equation method in a gas microchannel, *Phys. Rev. E,* 71 (2005) 046706.
[5] N. Jeong, C. L. Lin and D. H. Choi, Lattice Boltzmann study of three-dimensional gas microchannel flows, *J. Micromech. Microeng.,* 16 (2006) 1749-1759.
[6] S. A. Schaaf and P. L. Chambre, *Flow of rarefied gases,* Princeton University Press, Princeton, NJ (1961).
[7] G. A. Bird, *Molecular gas dynamics and the direct simulation of gas flows,* Oxford University Press, Clarendon (1994).
[8] E. B. Arkilic, M. A. Schmidt and K. S. Breuer, Gaseous slip flow in long microchannels, *J. Microelectromech. Syst.,* 6 (1997) 167-178.
[9] M. Sbragaglia and S. Succi, Analytical calculation of slip flow in lattice Boltzmann models with kinetic boundary conditions, *Phys. Fluids,* 17 (2005) 093602.
[10] Y. H. Zhang, R. Qin, Y. H. Sun, R. W. Barber and D. R. Emerson, Gas flow in microchannels – A Lattice Boltzmann method approach, *J. Stat. Phys.,* 121 (2005) 257-267.
[11] G. H. Tang, W. Q. Tao and Y. L. He, Lattice Boltzmann method for gaseous microflows using kinetic theory boundary conditions, *Phys. Fluids,* 17 (2005) 058101.
[12] Y. H. Qian, D. d'Humieres and P. Lallenmand, Lattice BGK models for Navier-Stokes equation, *Europhys. Lett.,* 17 (1992) 479-484.
[13] F. Sharipov and V. Seleznev, Data on internal rarefied gas flows, *J. Phys. Chem. Ref. Data,* 27 (1988) 657-706.
[14] J. C. Maxwell, On stress in rarefied gases arising from inequalities of temperature, *Philos. Trans. R. Soc.*, London, 170 (1879) 231-256.
[15] S. Ansumali and I. V. Karlin, Kinetic boundary conditions in the lattice Boltzmann method, *Phys. Rev. E,* 66 (2002) 026311.
[16] S. Succi, *The Lattice Boltzmann equation for fluid dynamics and beyond,* Oxford University Press, New York (2001).
[17] N. G. Hadjiconstantinou, Comment on Cercignani's second-order slip coefficient, *Phys. Fluids,* 15 (2003) 2352-2354.
[18] G. E. Karniadakis and A. Beskok, *Micro flows: Fundamentals and simulation,* Springer, New York (2002).
[19] Z. Guo, C. Zheng and B. Shi, Discrete lattice effects on the forcing term in the lattice Boltzmann method, *Phys. Rev. E,* 65 (2002) 046308.
[20] N. G. Hadjiconstantinou, Oscillatory shear-driven gas flows in the transition and free-molecular-flow regimes, *Phys. Fluids,* 17 (2005) 100611.
[21] C. Aubert and S. Colin, High-order boundary conditions for gaseous flows in rectangular microducts, *Microscale Thermophys. Eng.,* 5 (2001) 41-54.
[22] R. G. Deissler, An analysis of second-order slip flow and temperature jump boundary conditions for rarefied gases, *Int. J. Heat Mass Transfer,* 7 (1964) 681-694.
[23] G. H. Tang, Y. H. Zhang and D. R. Emerson, Lattice Boltzmann models for nonequilibrium gas flows, *Phys. Rev. E,* 77 (2008) 046701.
[24] G. H. Tang, X. J. Gu, R. W. Barber and D. R. Emerson, Lattice Boltzmann simulation of nonequilibrium effects in oscillatory gas flow, *Phys. Rev. E,* 78 (2008) 026706.
[25] T. Ohwada, Y. Sone and K. Aoki, Numerical analysis of the shear and thermal creep flows of a rarefied gas over a plane wall on the basis of the linearized Boltzmann equation for hard-sphere molecules, *Phys. Fluids A,* 1 (1989) 1588-1599.

Namgyun Jeong received his B.S., M.S. and Ph.D. degrees from the Division of Mechanical Engineering of KAIST in 1999, 2001 and 2007, respectively. His research is focused on computational fluid dynamics. He is currently a senior researcher at Korea Atomic Energy Research Institute in Korea.